CHEMISTRY OF MATERIALS

pubs.acs.org/cm

Article

A Complex Ternary Chromium Arsenide, $Eu_9Cr_{16}As_{19}$

Published as part of Chemistry of Materials special issue "Honoring the Outstanding Contributions of Mercouri Kanatzidis to Chemistry of Materials".

Kowsik Ghosh, Alexander Ovchinnikov, Michael O. Ogunbunmi, Shanta R. Saha, Johnpierre Paglione, and Svilen Bobev*

Cite This: *Chem. Mater.* 2025, 37, 9597−9608

Read Online

ACCESS | Metrics & More | Article Recommendations | Supporting Information

ABSTRACT: We report the results of extensive exploratory work in the Eu−Cr−As compositional space that led to the identification of hitherto unknown phase $Eu_9Cr_{16}As_{19}$. Its tetragonal crystal structure (space group $P4_2/mnm$; a = 15.2761(6) Å and c = 14.6014(8) Å) was established via single-crystal X-ray diffraction methods and boasts a high degree of complexity. The asymmetric cell consists of 21 symmetry-independent positions, including four Eu, nine Cr, and eight As, which account for a total of 176 atoms per unit cell (Pearson symbol $tP176$), with all atomic sites found to be fully occupied and with no indication of crystallographic disorder. Most of the Cr atoms are coordinated to five As atoms, and the $CrAs_5$ square-pyramids share common faces, edges, and corners to form an intricate array featuring a variety of Cr−Cr interactions. The temperature dependence of the magnetic susceptibility of polycrystalline $Eu_9Cr_{16}As_{19}$ is suggestive of a multifaceted magnetic structure that is yet to be determined. There are several observed transitions, and it is unclear which ones are contributed from the ordering of the Cr or Eu moments. In the paramagnetic regime, the calculated effective magnetic moment is close to the free-ion value of Eu^{2+}. Electronic structure calculations confirm that $Eu_9Cr_{16}As_{19}$ is a metallic system with a sizable reduction of the magnetic moments on the Cr atoms in their ground state.

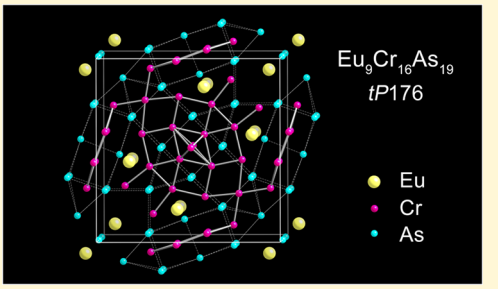

INTRODUCTION

Arsenides of the transition metals are extensively studied for their rich physical properties, such as unusual magnetism and/or unconventional superconducting behavior.[1] Chromium arsenides, specifically, have garnered significant attention.[2−7] For example, binary compound CrAs, which adopts an orthorhombic MnP-type structure, exhibits a noncollinear antiferromagnetic (AFM) ground state. Under external pressure exceeding 0.8 GPa, the AFM order is suppressed, giving rise to superconductivity at approximately 2 K.[6,8] Beyond binaries, a family of quasi-one-dimensional (quasi-1D) Cr-based superconductors, $A_2Cr_2As_3$ (A = Na, K, Rb, Cs),[2,3,5,7] has been discovered, exhibiting superconductivity at ambient pressure with a maximum superconducting transition temperature (T_C) of 8.6 K.[3] These compounds crystallize in a hexagonal structure, characterized by infinite $[Cr_3As_3]^{2-}$ double chains separated by the alkali metal cations. Notably, as the ionic radius of A^+ increases from Na^+ to Cs^+, T_C systematically decreases from 8.6 to 2.2 K.[2,3,5,7] Theoretical studies suggest that these quasi-1D Cr-based systems are in close proximity to a novel in−out coplanar magnetic ground state, with superconductivity intimately linked to the underlying magnetism.[9]

In addition to these superconducting arsenides, another family of ternary Cr-based compounds displays a range of magnetic properties.[10−12] All three members, $AECr_2As_2$ (AE = Sr, Ba, Eu), crystallize in the tetragonal $ThCr_2Si_2$-type structure. This atomic arrangement is known for the alternating CrAs layers composed of fused $CrAs_4$ tetrahedra, interleaved with AE layers along the c-axis. $SrCr_2As_2$ and $BaCr_2As_2$ exhibit itinerant G-type AFM ordering with remarkably high Néel temperatures of 590 and 580 K, respectively.[10,12] In comparison to its alkaline-earth metal analogs, $EuCr_2As_2$ demonstrates a more complex magnetic behavior due to competing ferromagnetic (FM) and AFM interactions.[11]

Besides the ternary chromium arsenides mentioned above,[2−5,7,9,10,12] there are also a few examples of lanthanide-containing Cr-based phases, which have been studied.[11,13] Quaternary systems with mixed As^{3-}, O^{2-}, and/or H^- anions also appear to have been investigated in the past, albeit sparsely. Considering the very large phase space available and

Received: October 7, 2025
Revised: November 14, 2025
Accepted: November 18, 2025
Published: December 1, 2025

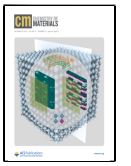

https://doi.org/10.1021/acs.chemmater.5c02660
Chem. Mater. 2025, 37, 9597−9608

the uptick in research interest in Fe-based arsenides, it is surprising that there are not more Cr-containing arsenides reported to date. Therefore, we sought to uncover unreported phases in these systems by undertaking exploratory work, and here, we present the first results from these studies—this article discusses the crystal structure and physical properties of $Eu_9Cr_{16}As_{19}$, a ternary Cr-arsenide containing europium, which can be considered as a "complex metallic alloy" (CMA).[14] In addition to the comprehensive structural characterization that was carried out based on single-crystal X-ray diffraction data, we also present preliminary data on the electronic structure and physical properties.

EXPERIMENTAL SECTION

Synthesis. Single crystals of $Eu_9Cr_{16}As_{19}$ were grown by the Sn flux method, and polycrystalline samples were made via solid-state direct reactions. All work was carried out under a protective inert atmosphere or under vacuum. The elements Eu, Cr, As, and Sn were purchased from Sigma-Aldrich and Alfa-Aesar with a purity of ≥99.9 wt % (metal basis). In the optimized flux-growth experiment, elemental mixtures were loaded in a 2 mL alumina crucible (with the ratio Eu/Cr/As/Sn = 10:16:22:40). Weighing of all elements was done in a glovebox filled with argon gas and actively controlled atmosphere (residual O_2 and H_2O below 1 ppm). The crucible was then topped with a piece of quartz wool and sealed in an evacuated fused silica tube. The sealed tube was then put into a muffle furnace for heat treatment as follows: (1) heating to 1123 K (rate 100 K/h); (2) equilibration at this temperature for 24 h; and (3) cooling to 873 K (rate 3 K/h). At that point, the tube was taken out from the muffle furnace, and the Sn flux was immediately separated from the crystalline material with the use of a centrifuge. Note that high-temperature centrifugation is associated with a risk of burns and must be performed with proper personal protective equipment: fireproof clothing, heat-resistant gloves, and a face shield. After that, the tube was transferred back to the glovebox and opened.

Polycrystalline sample of $Eu_9Cr_{16}As_{19}$ was synthesized by fusing the respective elements. A stoichiometric elemental mixture (total weight approximately 1 g) was put into a fused silica tube, which was subsequently evacuated and flame-sealed. The tube was then heated at 1223 K for 24 h before cooling to 873 K at a rate of 3 K/h, followed by cooling to room temperature at a rate of 100 K/h.

Structural Characterization. Powder X-ray diffraction (PXRD) measurements were taken at room temperature on a Rigaku Miniflex diffractometer (filtered Cu Kα radiation, λ = 1.5418 Å). Small portions of the obtained samples were ground into a powder using agate mortars and pestles. The data were collected between 20 and 60° in 2θ with a step size of 0.02° and 1 s per step counting time. PXRD measurements before and after exposure to air over 2 weeks were taken to confirm the stability of the phase in ambient conditions over this period of time (Figure S1). Considering the complexity of the crystal structure and large unit cell, Rietveld refinements were not feasible on the available PXRD data.

Suitable single crystals were selected and were cut under dry Paratone-N oil to appropriate dimensions (≤0.10 mm). After that, crystals were scooped by MiTeGen plastic loops and transferred to the goniometer of a Bruker APEX III diffractometer equipped with monochromatized Mo Kα radiation, λ = 0.71073 Å. Many crystals were screened by rapid scans before the best one was found. During the data collection, the crystal was kept under a stream of cold nitrogen (200(2) K). The data were collected and processed with the software packages supplied by Bruker.[15] The crystal structure was solved by the intrinsic phasing method using SHELXT and refined by full-matrix least-squares methods on F^2 with SHELXL.[16,17] Atomic coordinates were standardized using the STRUCTURE TIDY program.[18] Selected details of the data collection are given in Table 1.

Elemental Microanalysis. Metallographic analyses and elemental mapping were conducted on several crystals of $Eu_9Cr_{16}As_{19}$ from different batches to confirm their elemental compositions and the uniform distribution of the elements. The crystals were mounted on a carbon tape glued to an aluminum holder. The analyses were performed on an Auriga 60 Cross Beam Scanning Electron Microscope (SEM), equipped with an Oxford Instruments X-MAX80 energy-dispersive (EDX) spectrometer. The beam current was 10 μA at 20 kV accelerating potential. Data were collected over several spots, and the observed elemental proportions were consistent from sample to sample and were in agreement with the single-crystal X-ray diffraction work. The EDX result, SEM image, and elemental mapping figures are shown in Figure 1.

Table 1. Details of the Data Collection for $Eu_9Cr_{16}As_{19}$ (T = 200(2)) K; Mo Kα, λ = 0.71073 Å; Space Group $P4_2/mnm$ (No. 136), Z = 4

chemical formula	$Eu_9Cr_{16}As_{19}$
fw/g mol^{-1}	3623.12
a/Å	15.2761(6)
c/Å	14.6014(8)
V/Å^3	3407.4(3)
measured reflections	25501
independent reflections	2333
ρ_{calc}/g cm^{-3}	7.06
μ (Mo−Kα)/cm^{-1}	394.5
R_1 ($I > 2\sigma_{(I)}$)[a]	0.0246
wR_2 ($I > 2\sigma_{(I)}$)[a]	0.0447
$\Delta\rho_{max,min}$/e Å^{-3}	1.43, −1.33

[a] $R_1 = \sum||F_0| - |F_c||/\sum|F_0|$; $wR_2 = [\sum[w(F_0^2 - F_c^2)^2]/\sum[w(F_0^2)^2]]^{1/2}$, where $w = 1/[\sigma^2F_0^2 + (0.0060P)^2 + 38.3558P]$ and $P = (F_0^2 + 2F_c^2)/3$.

Electronic Structure Calculations. The electronic structure of $Eu_9Cr_{16}As_{19}$ was evaluated using the Stuttgart TB-LMTO-ASA code[19,20] within the local spin density approximation (LSDA). The von Barth-Hedin type of the LSDA functional was employed.[21] Empty spheres were introduced to satisfy the atomic sphere approximation (ASA). The Eu 4f orbitals were treated as core states. Initial spin polarization was applied to the Cr 3d states. For the final calculations, the Brillouin zone was sampled with an k-point step of about 0.07 Å^{-1}.

Magnetic Susceptibility Measurements. Temperature- and field-dependent magnetic measurements were carried out using a Quantum Design SQUID magnetometer MPMS3 in the temperature and field ranges of 2−300 K and 0−7 T, respectively. Approximately 45 mg of a polycrystalline $Eu_9Cr_{16}As_{19}$ sample was used, and it was enclosed in a gel cap. The $\chi(T)$ measurements were conducted in both zero-field-cooled (ZFC) and field-cooled (FC) modes. For the ZFC mode, the sample was cooled without applying a magnetic field; at the base temperature, a magnetic field was applied, and the magnetization was measured during the warming cycle. For the FC mode, after the application of a magnetic field, the magnetization was measured during the cooling cycle. For every measurement, the magnetic field was oscillated to zero before each measurement to minimize residual magnetic flux trapped in the superconducting solenoid.

Transport Property Measurements. High-temperature Seebeck coefficient measurements were carried out using the integral method, and a constantan wire was used as a reference on an SB-100 module MMR Tech. instrument. Multiple crystals (of appropriate geometry) from different batches were measured; each specimen was mounted on the platform by using a high-purity silver conductive paint interfaced with the probe by using the same silver conductive paint. During the whole process, the samples were exposed to air for only a very short duration of time. Data were gathered for temperatures ranging between 300 and 460 K, under a vacuum. To ensure the reproducibility of the results, the measurements were carried out in a heating and cooling mode cycle and repeated three times.

https://doi.org/10.1021/acs.chemmater.5c02660
Chem. Mater. 2025, 37, 9597−9608

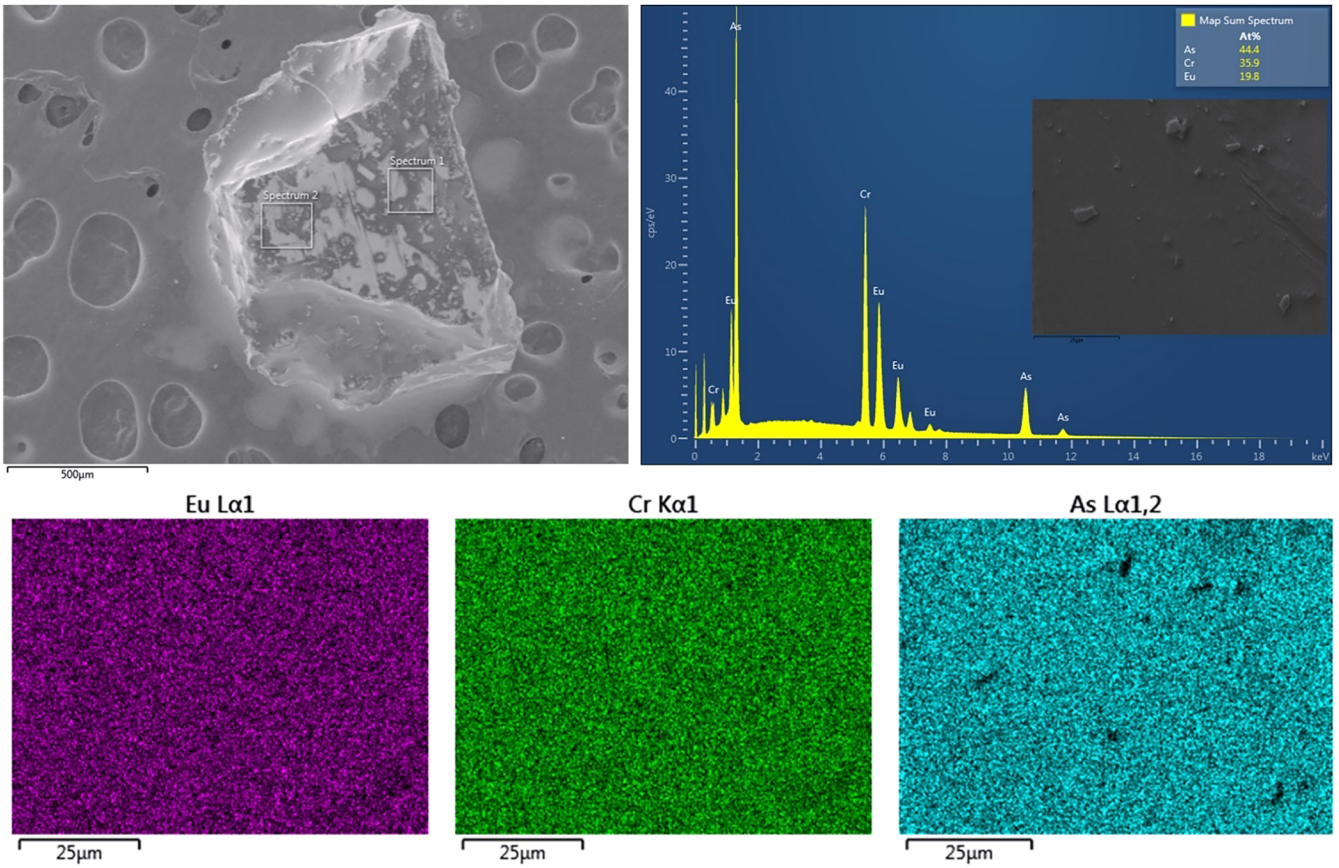

Figure 1. Scanning microscopy image (SEM), X-ray energy-dispersive spectrum, and elemental maps from EDX showing well-dispersed and homogeneously distributed Eu (purple), Cr (green), and As (blue) in $Eu_9Cr_{16}As_{19}$. The elemental analysis for $Eu_9Cr_{16}As_{19}$ yields the following values: 19.8 (Eu), 35.9 (Cr), and 44.4 (As), which are very close to those based on the chemical formula: 20.4 (Eu), 36.4 (Cr), and 43.2 (As). All quoted numbers are in atomic %.

RESULTS AND DISCUSSION

Synthesis. $EuCr_2As_2$ is the only example of ternary Cr-arsenide with europium that was known prior to this study.[11] $EuCr_2As_2$ can reportedly be easily synthesized by a solid-state reaction. At the same time, there are a number of reported binary Cr-arsenide[6,8,22−28] and Eu-arsenide[29−36] phases, Figure 2, although some of them appear to be accessible from high-pressure experiments.

Looking for new materials, we initially carried out a reaction with the elemental ratio Eu/Cr/As = 1:1:2, expecting to obtain

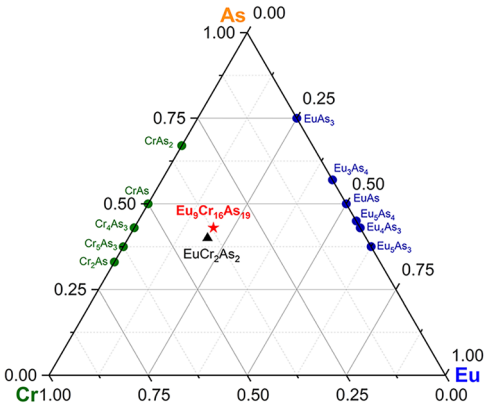

Figure 2. Schematic view of the compositional Eu−Cr−As diagram.

$EuCrAs_2$ analogous to the $EuZnSb_2$ phase we identified not too long ago.[37] This experiment yielded a few crystals that did not give diffraction patterns matching anything in the crystallographic databases; however, the crystal quality was not optimal, and this made the structure analysis through single-crystal X-ray diffraction methods difficult. The preliminary structural analysis of the sample resulted in an approximate chemical formula with much higher Cr contents. The complementary EDX spectroscopy results confirmed the atomic ratio close to the chemical formula from the SCXRD results (Figure 1).

Based on the approximate 1:2:2 ratio, we then carried out the Sn flux reaction described in the Experimental Section in order to grow better crystals. Indeed, such experiments were successful, allowing for the growth of crystals with a size of up to ca. 1 mm. The elemental mapping analyses of the crystals confirm that Sn is not in the chemical makeup of the synthesized materials and that the three elements are uniformly distributed homogeneously (Figure 1).

We should note that trial experiments to replace Sn- with Pb-flux were unsuccessful in producing the desired phase, likely because the solubility of Cr in liquid Pb at 1123 K is essentially zero. Similarly, attempts at analogues with Sb and Bi instead of As (and with different flux growths) were also unsuccessful. Keeping in mind the close ionic radii of Eu^{2+} (1.39 Å for CN 8) and Sr^{2+} (1.40 Å for CN 8),[38] an experiment to synthesize $Sr_9Cr_{16}As_{19}$ was also set up. The same heating procedure and

https://doi.org/10.1021/acs.chemmater.5c02660
Chem. Mater. 2025, 37, 9597−9608

Table 2. Atomic Coordinates and Equivalent Isotropic Displacement Parameter (U_{eq})[a] for $Eu_9Cr_{16}As_{19}$ from a Refinement of Single-Crystal X-ray Diffraction Data

atom	Wyckoff site	x	y	z	U_{eq}/Å^2
Eu1	16*k*	0.07334(2)	0.33380(2)	0.19433(2)	0.0063(1)
Eu2	8*j*	0.13499(2)	*x*	0.29851(3)	0.0091(1)
Eu3	8*j*	0.34649(2)	*x*	0.25294(3)	0.0071(1)
Eu4	4*f*	0.41951(3)	*x*	0	0.0093(1)
Cr1	16*k*	0.08341(6)	0.53109(6)	0.09210(7)	0.0053(1)
Cr2	8*i*	0.07060(9)	0.7277(1)	0	0.0065(1)
Cr3	8*i*	0.10719(9)	0.23095(9)	0	0.0041(1)
Cr4	8*i*	0.2121(1)	0.36501(9)	0	0.0069(1)
Cr5	8*i*	0.22551(9)	0.57362(9)	0	0.0062(1)
Cr6	4*g*	0.1053(1)	$\bar{x}$	0	0.0061(1)
Cr7	4*g*	0.2545(1)	$\bar{x}$	0	0.0062(1)
Cr8	4*f*	0.06711(9)	*x*	0	0.0047(1)
Cr9	4*e*	0	0	0.1401(1)	0.0060(1)
As1	16*k*	0.00313(4)	0.16640(4)	0.11588(4)	0.0051(1)
As2	16*k*	0.17300(4)	0.33672(4)	0.37423(4)	0.0057(1)
As3	16*k*	0.23363(4)	0.46828(4)	0.13142(4)	0.0059(1)
As4	8*j*	0.23291(4)	*x*	0.11120(6)	0.0057(2)
As5	8*i*	0.04171(6)	0.39463(6)	0	0.0044(2)
As6	4*g*	0.37539(6)	$\bar{x}$	0	0.0060(1)
As7	4*e*	0	0	0.31551(9)	0.0090(1)
As8	4*d*	0	1/2	1/4	0.0046(1)

[a]U_{eq} is defined as 1/3 of the trace of the orthogonalized U_{ij} tensor.

molten Sn as a flux were utilized, but the outcomes were different; the resulting phase(s) is(are) still unidentified.

Crystal Structure. Detailed analysis of the single-crystal X-ray diffraction pattern was consistent with tetragonal symmetry, and the reflection conditions 0*kl* for $k + l = 2n$, 0*k*0 for $k = 2n$, 00*l* for $l = 2n$, *h*0*l* for $h + l = 2n$, and *h*00 for $h = 2n$ suggested only three possible space groups: $P4_2/mnm$ (No. 136), $P\bar{4}n2$ (No. 118), and $P4_2nm$ (No. 102). Generation of the initial model was successful in the centrosymmetric space group $P4_2/mnm$ (No. 136). The complex crystal structure consists of a total of 21 crystallographic unique positions including four Eu, nine Cr, and eight As positions (Table 2), accounting for a total of 176 atoms per unit cell (Pearson symbol *t*P176). All positions were found fully occupied, with all refined atomic displacement parameters being nearly isotropic (Table 2). Final refinements yielded a flat difference Fourier map and low conventional residual factors (Table 1).

A schematic projection of the complex crystal structure of $Eu_9Cr_{16}As_{19}$, viewed down the [100] direction, is presented in Figure 3. There is no precedent for such a structure in the databases, meaning that this is the first time this atomic arrangement is being described. The structure can be considered as consisting of alternating thick (ca. 4 Å) slabs that are stacked along the [001] direction. While the slabs centered at approximately $z = 1/4$ and $z = 3/4$ consist of only Eu and As atoms, the ones centered around $z = 0$ and $z = 1/2$ are much more complicated and host all three types of atoms. Next, we describe each of them separately.

Figure 4 shows the slab that hosts all atoms, viewed down [001], where in panel a, we show only the topology of the Cr sublattice, and in panel b, we show only the Cr and As connectivity. For the sake of clarity, Eu atoms (Eu4) are omitted from the figure. The main structural unit can be immediately recognized, a square-pyramid of As atoms centered by the chromium atoms, which are typically found just above the base of the pyramids. This is the dominating

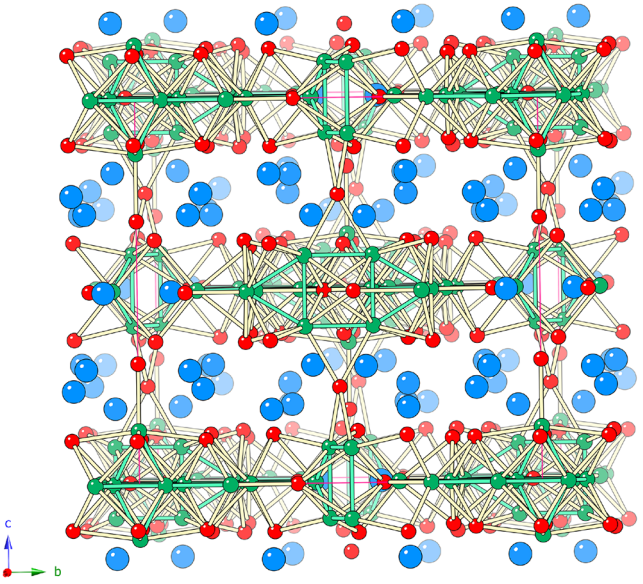

Figure 3. Crystal structure of $Eu_9Cr_{16}As_{19}$ in ball-and-stick representation, viewed in the [100] direction. The blue, green, and red colors represent Eu, Cr, and As atoms, respectively. The cylinders represent Cr−As contacts (<2.7 Å) and Cr−Cr contacts (<2.8 Å).

coordination mode of the Cr atoms (CN 5) with the exception of Cr6 and Cr8, which only have four nearest As neighbors. The latter, however, are not tetrahedrally positioned around the Cr centers (*vide infra*).

From the intricate topology of the Cr sublattice (Figure 4a), one might infer that the resultant Cr-centered square-pyramidal units must be joined in a very complicated manner (Figure 4b). Indeed, the $CrAs_5$ pyramids share common faces, edges, and corners to form an array in the *ab*-plane. There are two notable "protrusions" denoted with yellow shading in Figure 4b. The first protrusion from the slab is the tetramer

https://doi.org/10.1021/acs.chemmater.5c02660
Chem. Mater. 2025, 37, 9597−9608

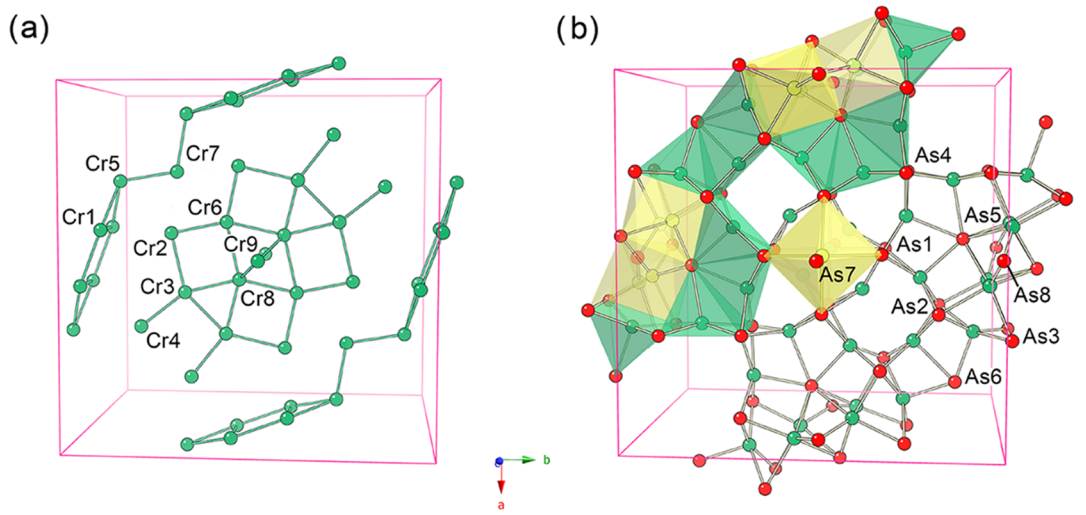

Figure 4. Cr sublattice in the crystal structure of $Eu_9Cr_{16}As_{19}$ (a); A combined ball-and-stick and polyhedral representation, showing the arrangement of fused square-pyramidal units (b). Cr6 and Cr8 are in a nearly square-planar coordination by As atoms. The chromium polyhedra shaded in yellow have As vertices that protrude into the Eu slabs above and below the Cr−As layers. Both panels are projections approximately down the [001] direction. The green (yellow) and red colors represent Cr and As atoms, respectively. The cylinders represent Cr−As contacts (d_{Cr-As} < 2.7 Å) and Cr−Cr contacts (d_{Cr-Cr} < 2.8 Å).

made up of four symmetry-equivalent Cr1 atoms, where two [$CrAs_5$] subunits share their triangular faces in the *ab*-plane; through further edge-sharing they are connected in an orthogonal direction (Figure 5a). The second is a "double-

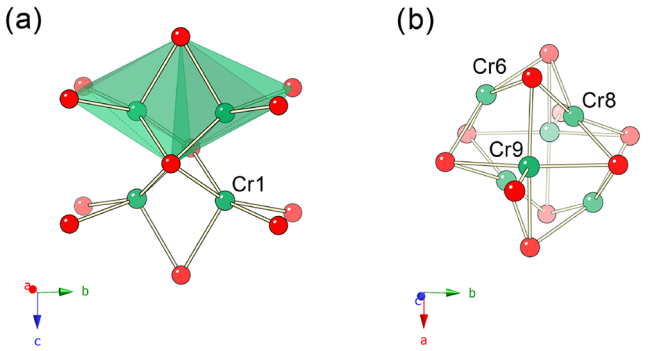

Figure 5. Close-up view of the tetrameric unit made up of four $Cr1As_5$ pyramids (a). Close-up view of the hexameric unit made up of two $Cr9As_5$ pyramids, two $Cr6As_4$, and two $Cr8As_4$ square fragments (b). The green and red colors represent Cr and As atoms, respectively.

pyramidal unit" which is the construct of two [$Cr9As_5$] pyramids facing in opposite directions along [001], which are bridged by two Cr6 and two Cr8 atoms.

One should notice that both the Cr6 and Cr8 atoms are coordinated to As atoms in nearly square-planar geometry (Figure 5b), although the actual coordination number of the Cr6 and Cr8 atoms is higher than 4 due to the close proximity of Cr neighbors. A similar coordination environment of a Cr atom exists in the structure of the binary phase Cr_4As_3 (Figure S3).[23] We further note that examples of solid-state structures with Cr atoms in (near) square-planar coordination are not common; with the Cr^{2+}−based silicate pigments reported by Subramanian et al.,[39] being among the most widely known square-planar cases.

The range of Cr−As distances in $Eu_9Cr_{16}As_{19}$ is wide. The Cr−As distances for the Cr atoms with CN 5 range from ca. 2.42 to ca. 2.68 Å (Table 3). The longest d_{Cr-As} are the distances from Cr to the apical As atoms. The average d_{Cr-As}

Table 3. Selected Interatomic Distances (Å) in $Eu_9Cr_{16}As_{19}$

atom 1	atom 2	distance	atom 1	atom 2	distance
Cr1	As2	2.536(1)	Cr8	As1 (4×)	2.474(1)
	As3	2.553(1)		Cr9 (2×)	2.507(2)
	As5	2.561(1)		Cr3 (2×)	2.577(2)
	As5	2.598(1)			
	As8	2.677(1)	Cr9	As7	2.561(2)
	Cr5	2.635(1)		As1 (4×)	2.567(1)
				Cr8 (2×)	2.507(2)
Cr2	As2 (2×)	2.465(1)			
	As5	2.537(2)	Eu1	As8	2.8917(3)
	As1 (2×)	2.598(1)		As1	3.0009(7)
	Cr6	2.606(2)		As5	3.0252(5)
				As2	3.0353(7)
Cr3	As4 (2×)	2.515(1)		As4	3.1288(7)
	As1 (2×)	2.522(1)		As3	3.1800(7)
	As5	2.693(2)		As3	3.3253(7)
	Cr8	2.577(2)			
	Cr4	2.600(2)	Eu2	As7	2.9274(3)
				As6	2.9510(5)
Cr4	As3 (2×)	2.505(1)		As2 (2×)	3.3247(7)
	As4 (2×)	2.610(1)		As1 (2×)	3.3759(7)
	As5	2.642(2)		As3 (2×)	3.4004(7)
	Cr3	2.600(2)		As4	3.4569(9)
Cr5	As6	2.418(2)	Eu3	As1 (2×)	3.0707(7)
	As3 (2×)	2.508(1)		As3 (2×)	3.0954(7)
	As2 (2×)	2.566(1)		As2 (2×)	3.1912(7)
	Cr1 (2×)	2.635(1)		As4	3.2102(8)
	Cr7	2.662(2)		As7	3.4634(5)
Cr6	As1 (4×)	2.545(1)	Eu4	As6 (2×)	3.205(1)
	Cr2 (2×)	2.606(2)		As7 (2×)	3.206(1)
				As3 (4×)	3.5066(7)
Cr7	As2 (4×)	2.558(1)			
	As6	2.611(2)			
	Cr5 (2×)	2.662(2)			

https://doi.org/10.1021/acs.chemmater.5c02660
Chem. Mater. 2025, 37, 9597−9608

value of 2.55 Å matches almost perfectly the sum of the elemental radii (r_{Cr} = 1.39 Å; r_{As} = 1.19 Å),[40] indicative of the presence of strong covalent bonding. For the two Cr atoms with CN 4, the d_{Cr-As} contacts are in the much narrower range from 2.48 to 2.55 Å (Table 3). The average value of the Cr−As distances in $Eu_9Cr_{16}As_{19}$ is comparable with the d_{Cr-As} = 2.50(1)−2.55(1) Å in Cr_2As,[25] and d_{Cr-As} = 2.53(1)−2.56(1) Å in Cr_5As_3.[24] The structures of these binaries are with the tetragonal space group *P4/nmm* (Figure S2a) and the orthorhombic space group *Pnma*, respectively (Figure S2b), and feature Cr atoms with CN 5 in pyramidal geometry. Another relevant example is the previously mentioned structure of Cr_4As_3 (space group *Cm*), in which seven of the eight crystallographically unique Cr atoms are either pyramidally or octahedrally coordinated by As (Figure S3).[23] The average d_{Cr-As} values in the Cr_4As_3 structure are 2.49(1) Å for CN 4, and increase to d_{Cr-As} = 2.53(1) Å for CN 6. In $EuCr_2As_2$,[11] the only other ternary europium chromium arsenide (Figure S4), d_{Cr-As} = 2.46(1) Å. One should notice that in the latter structure, all Cr atoms are tetrahedrally coordinated by As.

The slabs that host all of the Cr and most of the As atoms also host the Eu4 atoms, as shown in Figure 6. The coordination environment is with CN 8 in the form of a square antiprism, with some of the Eu−As distances as long as the Eu4−Eu4 separation, which measures 3.478(1) Å.

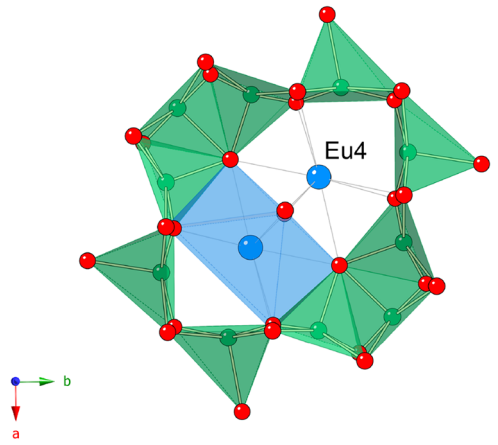

Figure 6. Local coordination environment of the Eu4 atoms. Eu4−Eu4 separation is ca. 3.48 Å.

The slabs centered around z = 1/4 and z = 3/4 consist of only Eu and As atoms and are comparatively simpler (Figure 7). The Eu1 atoms have irregular polyhedra of 7 nearest As atoms around them with $d_{Eu1-As8}$ being 2.89(1) Å, which is the shortest Eu−As contact in the structure. Such values are not without a precedent, and match well with as d_{Eu-As} = 2.9 Å in EuAs,[34] a binary arsenide with the Na_2O_2-type structure. The second shortest ones are $d_{Eu2-As7}$ = 2.93(1) Å and $d_{Eu2-As6}$ = 2.95(1) Å (Table 3), although the Eu2 atoms have larger polyhedra of the 9 nearest As atoms around them. The Eu2 polyhedra are more symmetric and have the shape of monocapped square antiprisms with an average Eu−As distance greater than 3.1 Å. Eu3 atoms have a coordination environment with CN 8, in the form of square antiprism (Figure 7b), with the shortest $d_{Eu3-As1}$ = 3.07(1) Å and $d_{Eu3-As3}$ = 3.10(1) Å (Table 3). Such values compare well with the Eu−As distances in Eu_5As_4 (ca. 3.1 Å),[32] Eu_5As_3 (ca. 3.04 Å),[35] $EuAs_3$ (ca. 3.05 Å),[31] Eu_4As_3 (ca. 3.04 Å),[33] and close to the sum of the elemental radii (r_{Eu} = 1.98 Å; r_{As} = 1.19 Å).[40] The rest of the d_{Eu-As} values in $Eu_9Cr_{16}As_{19}$ are on par or slightly longer than the Eu−As distances in $EuCr_2As_2$ (3.22 Å), where the Eu atoms are also coordinated by eight As atoms (Figure S4).[11] The wide range of d_{Eu-As} values is suggestive of the Eu−As bonding as being intermediate between covalent and ionic.

Electronic Structure. Due to the complexity of the $Eu_9Cr_{16}As_{19}$ crystal structure, a number of simplifications were employed. The first one was with regard to treating the Eu states. Assuming that the Eu cations in $Eu_9Cr_{16}As_{19}$ are likely present predominantly, or completely, in the 2+ state, one should consider them as magnetic ions with electron configuration $4f^7$. This requires performing calculations for different starting magnetic arrangements of the Eu^{2+} magnetic moments. In addition, strong electronic correlations of the 4f electrons have to be taken into account, which is often done by treating the 4f states with the LDA + *U* method.[41] Since such calculations are hardly feasible for such a complex material, we treated the Eu 4f orbitals as core states. With the 4f orbitals being usually highly localized, this simplification is not expected to have a major impact on the calculation results, aside from these states ending up missing from the calculated electronic structure. While this approach is widely used for compounds of rare-earth metals, we should note that some important details, such as potential mixed valence of Eu, occasionally reported for pnictides,[42,43] cannot be captured when this approximation is used.

With the Eu 4f orbitals being treated as core states, the only magnetic species to be taken into account in $Eu_9Cr_{16}As_{19}$ is Cr. This is the second major point of consideration that required simplification, since there are 9 symmetry-unique Cr sites in the structures, resulting in a total of 64 Cr atoms per unit cell. Even without constructing additional supercells, this leads to 2^{64} possible magnetic structures to consider (of course, this number is strongly overestimated since many such magnetic structures will be equivalent by symmetry). Therefore, in this contribution, we only study the case with a ferromagnetic starting spin arrangement.

At first, the energy and electron density of $Eu_9Cr_{16}As_{19}$ were calculated for a nonspin-polarized case with a *k*-point grid of 2 × 2 × 2. After that, the converged density was used as the starting electron density for spin-polarized calculations on the same *k*-point grid. The starting magnetic moments on all Cr atoms were set to 2 μ_B. Finally, for an accurate density of states (DOS) evaluation, spin-polarized calculations were carried out with a denser *k*-point grid of 4 × 4 × 4, starting from the electron density obtained in the previous round of calculations.

The magnetic moments on the Cr atoms converged to the following values (in μ_B): Cr1 −1.894, Cr2 −1.926, Cr3 1.460, Cr4 −2.046, Cr5 1.370, Cr6 1.663, Cr7 −2.118, Cr8 −1.133, and Cr9 0.929. Interestingly, despite the fact that the calculations were started from a ferromagnetic structure, the resulting magnetic arrangement is ferrimagnetic. Of course, the found magnetic structure is likely not the actual magnetic ground state of $Eu_9Cr_{16}As_{19}$ but rather a local energy minimum in the vicinity of the starting ferromagnetic arrangement. However, the fact that the starting ferromagnetic alignment is not retained after convergence of the self-consistent cycles suggests strong inherent antiferromagnetic interactions in the Cr substructure, which stabilize antiparallel alignment for some of the magnetic moments.

https://doi.org/10.1021/acs.chemmater.5c02660
Chem. Mater. 2025, 37, 9597−9608

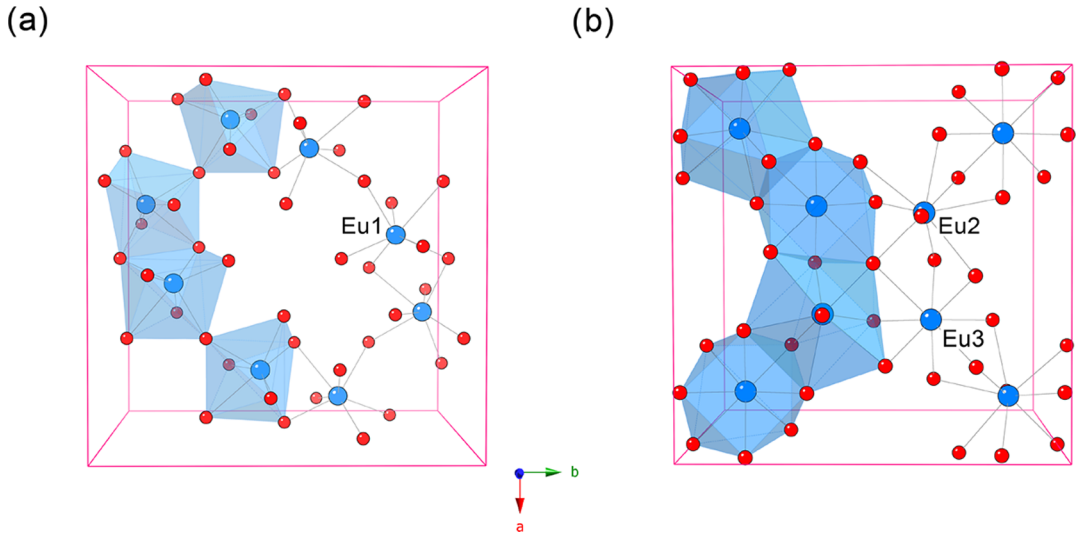

Figure 7. (a) Local coordination of the Eu1 atoms. (b) Local coordination of the Eu2 and Eu3 atoms.

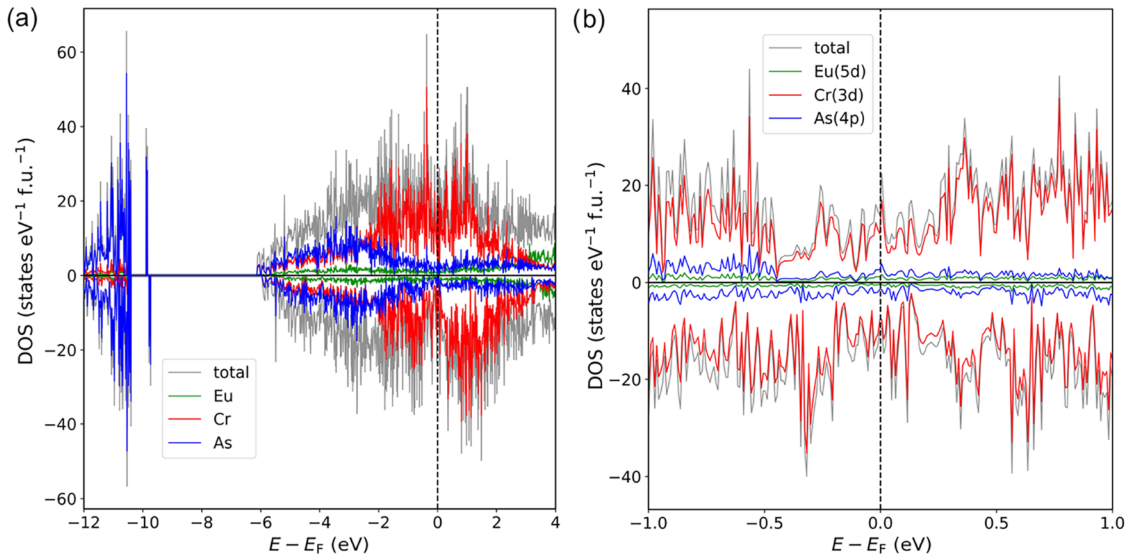

Figure 8. (a) Total and projected electron density of states (DOS) of $Eu_9Cr_{16}As_{19}$. Positive and negative DOS values correspond to the major and minor spin channels, respectively. (b) Close-up view of the DOS near the Fermi level with the dominant orbital contributions indicated.

The average charge of the Cr ions can be estimated from the formula $Eu_9Cr_{16}As_{19}$, considering that all As atoms should be assigned as isolated As^{3-} anions due to the lack of any As−As bonds. As discussed already, the Eu cations are presumed all to be Eu^{2+}, which yields a value of 2.44+ per Cr ion. A more structure-based, site-specific estimation can be obtained by using the bond-valence sum method,[44,45] with the tabulated parameters from ref 45. This approach gives the following bond-valence-sum values for the Cr sites: Cr1 2.6, Cr2 3.01, Cr3 2.88, Cr4 2.69, Cr5 3.18, Cr6 2.35, Cr7 2.7, Cr8 2.81, and Cr9 2.72.

Both estimations suggest that the formal charge of Cr is close to 3+, which corresponds to a magnetic moment of 3 μ_B (in the absence of strong splitting of the Cr *d*-orbitals by the crystal field). The significantly reduced magnetic moments of the Cr atoms found in our calculations point toward electronic delocalization or quenching of the localized magnetism via formation of metal−metal bonds. It is worth noting that the ordered magnetic moment of Cr in $EuCr_2As_2$, determined by neutron diffraction at 2 K, was also found to be highly reduced in comparison with the theoretical high-spin value due to itinerant antiferromagnetism.[11,46]

The electronic density of states for $Eu_9Cr_{16}As_{19}$ is shown in Figure 8. Low-lying states below about $E - E_F = -9$ eV are dominated by the As 4s contribution, in line with the presence of electron lone pairs on the As atoms. Close to E_F, the Cr 3d states are prevailing. Due to the large number of atomic sites (and hence, basis set orbitals) in the structure, the DOS around the Fermi level is highly structured and displays a number of narrow peaks. The Fermi level crosses one of those peaks (Figure 8b), which may indicate possible magnetic instability. In this case, it likely suggests that a more favorable magnetic arrangement exists with reduced DOS at E_F.

All in all, our calculations show that $Eu_9Cr_{16}As_{19}$ is a metallic system with a complex magnetic structure, which is yet to be determined, and a sizable reduction of magnetic moments on the Cr atoms. The effect of the magnetic Eu substructure on the overall magnetism of this phase, as well as potential implications of the uncovered antiferromagnetic interactions in

https://doi.org/10.1021/acs.chemmater.5c02660
Chem. Mater. 2025, 37, 9597−9608

the Cr substructure, such as the possibility of magnetic frustration, should become subjects for future studies.

Magnetic Response. The temperature dependence of the magnetic susceptibility for a polycrystalline $Eu_9Cr_{16}As_{19}$ sample measured under magnetic fields of 0.1 and 1 T is shown in Figure 9. At temperatures above 250 K, the sample exhibits a paramagnetic behavior, which is also confirmed by isothermal magnetization measurements (Figure 10). Several magnetic transitions are discernible between 2 and 250 K, which can be especially well visualized by plotting the temperature-dependent data in the $d(\chi T)/dT$ form (Fisher's heat capacity, Figure 9, inset).

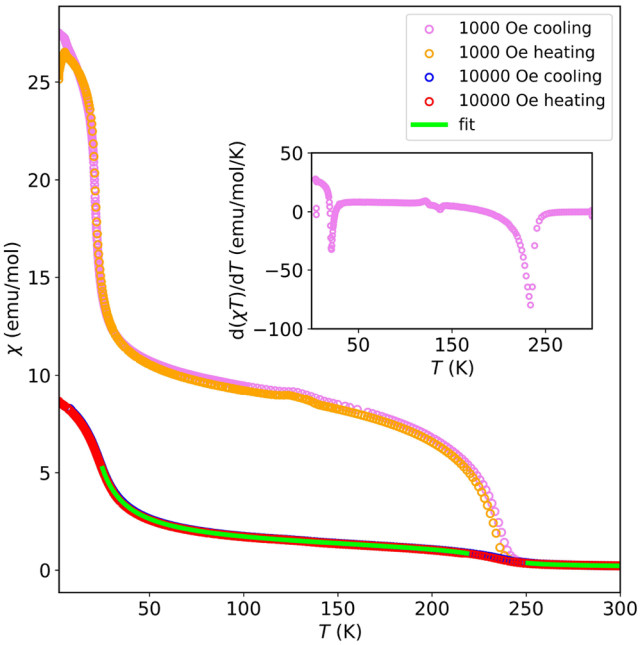

Figure 9. Temperature dependence of the magnetic susceptibility for $Eu_9Cr_{16}As_{19}$.

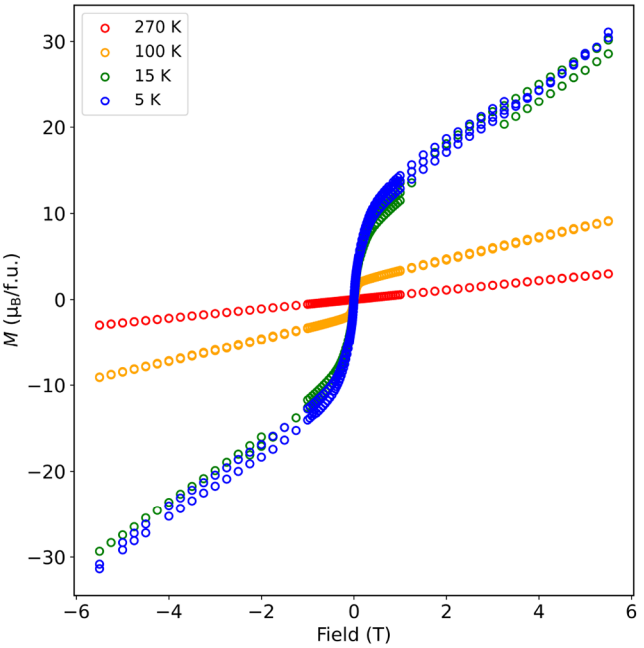

Figure 10. Isothermal magnetization of $Eu_9Cr_{16}As_{19}$ measured at four different temperatures.

Upon cooling, the first apparent magnetic transition takes place below 234 K, accompanied by a sharp increase in the magnetic susceptibility with decreasing temperature. This ferromagnetic-like transition may be of intrinsic origin, and in such a case, it should putatively be attributed to the Cr sublattice. However, a similar transition was observed in multiphase samples of complex chromium arsenides,[47,48] where it was ascribed to the presence of a ferromagnetic impurity, presumably Cr_4As_3 (which must be identical to the arsenide referred to as "Cr_3As_2" in the old literature[49]). The latter phase was reported to order ferromagnetically at about 250 K, but deviations from ideal stoichiometry can affect the transition temperature.[49] In the absence of heat capacity measurements and/or magnetic susceptibility of the single-crystalline specimen, we cannot conclude whether the transition at 234 K is intrinsic to the $Eu_9Cr_{16}As_{19}$ phase.

Upon further decrease of the temperature, another kink in the $\chi(T)$ data occurs at about 123 K. This feature is partially obscured by the ferromagnetic-like contribution developed below 234 K. In addition, the 123 K transition becomes less pronounced at higher magnetic fields. Below 21 K, a slight bifurcation between the zero-field-cooled (ZFC) and field-cooled (FC) susceptibility curves is visible under an applied magnetic field of 0.1 T. This temperature is very close to the ferromagnetic transition in the Eu sublattice of $EuCr_2As_2$,[11,46] which could be present as an impurity phase in our sample. Finally, below 5 K, an antiferromagnetic-like transition occurs, likely corresponding to magnetic ordering in the Eu sublattice of $Eu_9Cr_{16}As_{19}$. It is worth noting that at all temperatures below 234 K, a noticeable paramagnetic component is retained, likely associated with the magnetic Eu species. This assumption is further corroborated by the fitting of the data, as discussed below.

Due to a very narrow paramagnetic region in our measurements (250 K < T < 300 K), it was not possible to reliably extract the magnetic moment from the high-temperature data. Instead, we used a two-region model to fit the data. At temperatures between 25 and 220 K, the magnetic susceptibility data are fitted using the equation

$$\chi(25\ \mathrm{K} < T < 220\ \mathrm{K}) = \chi_0 + C_1/(T - \Theta_1) + (m/H)(1 - T/T_C)^{\beta} \quad (1)$$

where the first term is the temperature-independent contribution, the second term describes the paramagnetic species still present in this temperature region, while the third term reproduces the temperature evolution of the ferromagnetic-like component below T_C. The m parameter in the equation is the saturation moment, and the β parameter is the critical exponent. In this description, it is assumed that the paramagnetic species are independent of the ferromagnetic component, which is a somewhat crude approximation.

At temperatures above 250 K, the magnetic susceptibility is described by the following equation

$$\chi(T > 250\ \mathrm{K}) = \chi_0 + C_1/(T - \Theta_1) + C_2/(T - \Theta_2) \quad (2)$$

The first two terms in this equation are the same as for the low-temperature part since these contributions are expected to be present in the high-temperature region as well. The third

https://doi.org/10.1021/acs.chemmater.5c02660
Chem. Mater. 2025, 37, 9597−9608

term describes any additional paramagnetic species that undergo magnetic ordering upon cooling below 250 K.

Since the behavior of the susceptibility curve is difficult to describe in the near vicinity of magnetic transitions, the temperature region between 220 and 250 K was not considered. Furthermore, only the data measured at 1 T were used for fitting, because the contribution of the 123 K transition in those data was hardly visible and could be ignored for the purpose of the fitting. Both temperature regions were fitted simultaneously. To prevent the fitted parameters from ending up at a local minimum, global optimization was applied. Three different global optimization algorithms were used: differential evolution, dual annealing, and covariance matrix adaptation evolution strategy (CMA-ES).[50,51] For each of the three methods, the fitting was repeated five times, starting from random parameters. In all runs and across all used algorithms, the fitted parameters converged to the same solution, indicating that a global minimum was likely found. After the global optimization step, the parameters were additionally optimized locally. The resulting fit is shown as a solid line in Figure 9.

The fit yielded the following values: $\chi_0 = -0.00959$ emu/mol, $C_1 = 56.828$ (emu K)/mol, $\Theta_1 = 10.8$ K, $m = 5.169\ \mu_B$/f.u, $T_C = 228.7$ K, $\beta = 0.23$, $C_2 = 1.966$ (emu K)/mol, and $\Theta_2 = 236.07$ K. The C_1 value corresponds to a magnetic moment of 21.32 μ_B/f.u. or 7.11 μ_B/Eu. This moment is slightly lower than the theoretical value of 7.94 μ_B for free-ion Eu^{2+}. The origins of this apparent moment reduction are not clear yet; it could be due to impurities in the sample, although the presence of some amounts of Eu^{3+} in $Eu_9Cr_{16}As_{19}$ and potential mixed-valent behavior cannot be completely ruled out. It is worth noting that the reported magnetic moment of Eu in the compositionally similar $EuCr_2As_2$ is 7.07 μ_B,[46] which is also smaller than the expected value for free-ion Eu^{2+}. Furthermore, the ordered moment of Eu in $EuCr_2As_2$ determined by neutron diffraction also appears to be smaller than the theoretical value for Eu^{2+} (6.2 μ_B instead of 7.0 μ_B).[46] Whether partial contributions from crystal electric field effects or the presence of any amounts of Eu^{3+} in $Eu_9Cr_{16}As_{19}$ (and $EuCr_2As_2$), which could explain the observed reduction of the moment, remains to be determined. It is clear, however, that in our $Eu_9Cr_{16}As_{19}$ sample, the paramagnetic component between 25 and 220 K is associated solely with the Eu species, since any additional paramagnetic contributions would lead to a higher value of the observed magnetic moment. The Θ_1 value can then be interpreted as the Weiss temperature for the Eu sublattice. The small magnitude of the fitted Weiss constant is consistent with the low ordering temperature of 5 K. The positive sign of the Weiss constant suggests dominant ferromagnetic interactions. While the transition at 5 K appears to be of an antiferromagnetic type, the increasing bifurcation of the ZFC and FC susceptibility curves with decreasing temperature, visible in the 0.1 T data, points to some uncompensated magnetic moment, possibly in the form of canted antiferromagnetism, which would be consistent with the presence of some ferromagnetic exchange suggested by the Weiss constant.

Above 250 K, in addition to the paramagnetic Eu component, another Curie–Weiss term is present with a fitted C_2 value of 1.966 (emu K)/mol, corresponding to 3.97 μ_B/f.u. or 0.99 μ_B/Cr. Interestingly, the fitted Weiss constant, 236.07 K, is close to the observed ferromagnetic-like transition temperature and has a positive sign, suggesting a leading ferromagnetic exchange. Two explanations can be given to the observed values. The first possibility is that the Cr sublattice in $Eu_9Cr_{16}As_{19}$ stays paramagnetic above 250 K, but undergoes a magnetic ordering at lower temperatures. The relatively small magnetic moment per Cr atom is in line with our first-principle predictions.

The second possible explanation is that the Cr species in $Eu_9Cr_{16}As_{19}$ order antiferromagnetically above 300 K, while the paramagnetic component with a small magnetic moment at temperatures between 250 and 300 K is due to paramagnetic impurities only. The 234 K transition is then likely associated with an impurity as well. At the moment, it is not possible to distinguish between these two possibilities. Larger single crystals or single-phase powder specimens will be needed for further analysis. Once such samples are available, high-temperature magnetization and Mössbauer spectroscopy measurements can be carried out to gain a deeper insight into the magnetism of $Eu_9Cr_{16}As_{19}$.

Transport Properties. Due to the difficulty in synthesizing sizable single crystals for a detailed investigation of its intrinsic transport properties, we only present the preliminary Seebeck coefficient $S(T)$ for $Eu_9Cr_{16}As_{19}$. The measurement was carried out on a single crystal with a longest dimension of about 1.5 mm and in the temperature range of 300–460 K. As shown in Figure 11, $S(T)$ of $Eu_9Cr_{16}As_{19}$ varies from a room

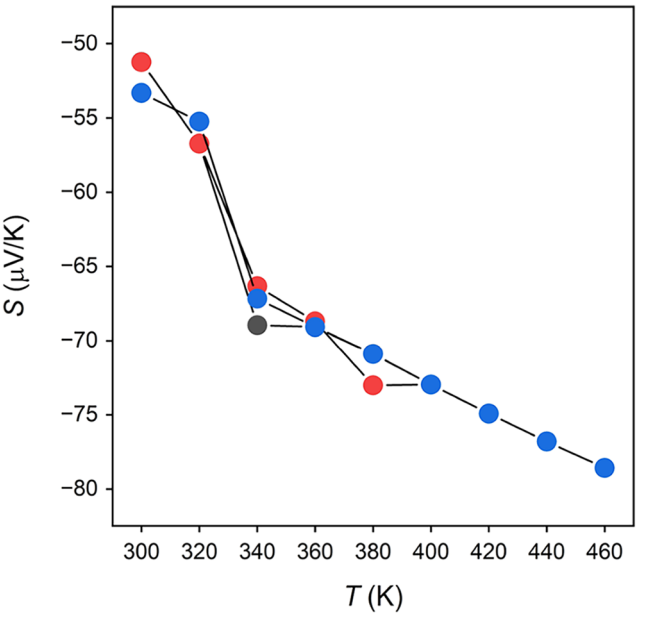

Figure 11. Evolution of the Seebeck coefficient of $Eu_9Cr_{16}As_{19}$ with the temperature. The different color dots represent the data from three independent measurements.

temperature value of ca. −50 μV/K at 300 K to ca. −80 μV/K at 460 K, showing an increase of nearly 63% in magnitude in the small temperature range measured. At around 340 K, a change in slope can be observed, although the origin of such an observation is not immediately clear. Here, we also note that $S(T)$ is negative throughout the temperature range studied, suggesting that the electrons are the dominant charge carriers and are involved in the heat transfer mechanism. Additionally, at 460 K, it is noted that $S(T)$ is still a decreasing function of T, with no visible sign of saturation or excitation of minority charge carriers. As such, |

https://doi.org/10.1021/acs.chemmater.5c02660
Chem. Mater. 2025, 37, 9597−9608

$S(T)$| is expected to attain a magnitude much higher at elevated temperatures.

The calculated electronic structure and the DOS presented in Figure 8 are supported by the $S(T)$ data, as for a system which is metallic, one would not normally observe a large magnitude |$S(T)$|.[52] Yet, the observed $Eu_9Cr_{16}As_{19}$ room temperature value is an order of magnitude higher than those of simple metals, and it is akin to those of degenerately doped semiconductors.[52,53] Recently, enhanced $S(T)$, with dominant electron carriers as found in the title phase, have also been reported in some Fe- and Mn-based oxyarsenides,[54,55] which are being explored as a potential *n*-type thermoelectric material. In this regard, the title compound holds great promise, as its thermoelectric transport properties could be optimized through an appropriate doping mechanism. We also speculate that if a suitable approach to dope $Eu_9Cr_{16}As_{19}$ can be identified, it may further provide for a useful materials platform to study superconductivity, which is ubiquitous in chromium-arsenide phases.[56,57]

One should recall that the DOS curve (Figure 8) is simplified by treating the 4f electrons as core states, thus precluding the observation of possible hybridization of the localized 4f with the conduction electrons near the Fermi level. Based on the $S(T)$ and the DOS results, one can expect the electrical resistivity to evolve in a metallic manner, and subsequent studies are expected to provide more insight into this. Such studies are also expected to unravel the nature of the lattice thermal conductivity of the title phase, since its intricate atomic bonding and the large unit cell volume reported here are known to drive an ultralow lattice thermal conductivity.[58−62] Recent studies have also demonstrated the role of magnetism-mediated thermoelectric transport properties,[61−65] and it remains to be seen how the magnetic order parameter observed in the title phase will affect its transport properties within the ordered temperature range.

CONCLUSIONS

In this report, we present the synthesis and structural characterization of $Eu_9Cr_{16}As_{19}$, the second only ternary chromium arsenide with europium known so far. Crystals were grown by the molten tin flux method, and the complex crystal structure was established through single-crystal X-ray diffraction methods. Electronic structure calculations indicate a metallic system, which was further validated experimentally by thermopower measurements. While multiple magnetic transitions were noticed, low-temperature magnetic ordering below 5 K can be related to the antiferromagnetic ordering of Eu^{2+} with a lower magnetic moment value compared to the theoretical value for a free-ion $4f^7$ ground state. It is still unclear whether the paramagnetic contribution above 250 K is from the Cr^{3+} ions or from impurities. The effect of the magnetic Eu substructure on the overall magnetism of this phase, as well as potential implications of the uncovered antiferromagnetic interactions in the Cr substructure, such as the possibility of magnetic frustration, should become subjects for future studies.

From the preliminary characterization discussed in the article, it is apparent that this new arsenide exhibits intricate structural characteristics, and it presents us with yet another material's playground system to explore the interplay between structural, electronic, and magnetic degrees of freedom that may be of great interest and beneficial for various applications. As such, growing larger single crystals would be desired for future studies. Coupled with that, high-temperature magnetization and Eu Mössbauer spectroscopy measurements can provide some clarity regarding the magnetic behavior of the 4f and 3d metal ions in this system. An approach by replacing Eu atoms with nonmagnetic Sr seems plausible, and can be suggested as another follow-up work for the future, which could potentially yield an isostructural $Sr_9Cr_{16}As_{19}$ phase with a simplified magnetic structure. It would also be revealing to study the effects of the possible magnetic correlations and their effect on the transport properties.

ASSOCIATED CONTENT

Supporting Information

The Supporting Information is available free of charge at https://pubs.acs.org/doi/10.1021/acs.chemmater.5c02660.

It includes powder X-ray diffraction pattern of $Eu_9Cr_{16}As_{19}$ (before and after exposure to air, Figure S1); representations of the crystal structures of Cr_2As (Figure S2a), Cr_5As_3 (Figure S2b), Cr_4As_3 (Figure S3), and $EuCr_2As_2$ (Figure S4) (PDF)

Accession Codes

Deposition Number 2487093 contains the supplementary crystallographic data for this paper. These data can be obtained free of charge via the joint Cambridge Crystallographic Data Centre (CCDC) and Fachinformationszentrum Karlsruhe Access Structures service.

AUTHOR INFORMATION

Corresponding Author

Svilen Bobev − *Department of Chemistry and Biochemistry, University of Delaware, Newark, Delaware 19716, United States;* orcid.org/0000-0002-0780-4787; Email: bobev@udel.edu

Authors

Kowsik Ghosh − *Department of Chemistry and Biochemistry, University of Delaware, Newark, Delaware 19716, United States;* orcid.org/0000-0003-2622-7046

Alexander Ovchinnikov − *Department of Chemistry and Biochemistry, University of Delaware, Newark, Delaware 19716, United States; Faculty of Chemistry and Food Chemistry, Technische Universität Dresden, 01062 Dresden, Germany*

Michael O. Ogunbunmi − *Department of Chemistry and Biochemistry, University of Delaware, Newark, Delaware 19716, United States; Department of Physics and Computer Science, Xavier University of Louisiana, New Orleans, Louisiana 70125, United States*

Shanta R. Saha − *Maryland Quantum Materials Center, Department of Physics, University of Maryland, College Park, Maryland 20742, United States*

Johnpierre Paglione − *Maryland Quantum Materials Center, Department of Physics, University of Maryland, College Park, Maryland 20742, United States*

Complete contact information is available at: https://pubs.acs.org/10.1021/acs.chemmater.5c02660

Author Contributions

The manuscript was written through the contributions of all authors. All authors have given approval to the final version of the manuscript.

Funding

The authors acknowledge financial support from the US DOE, under award #DE-SC0008885. Research at the University of Maryland was supported by the Gordon and Betty Moore Foundation's EPiQS Initiative through Grant No. GBMF9071, the U.S. National Science Foundation (NSF) Grant No. DMR2303090, and the Maryland Quantum Materials Center. S.R.S. acknowledges support from the National Institute of Standards and Technology Cooperative Agreement 70NANB17H301.

Notes

The authors declare no competing financial interest.

REFERENCES

(1) Kamihara, Y.; Watanabe, T.; Hirano, M.; Hosono, H. Iron-Based Layered Superconductor La[$O_{1-x}F_x$]FeAs (x = 0.05−0.12) with T_c = 26 K. *J. Am. Chem. Soc.* **2008**, *130*, 3296−3297.

(2) Tang, Z. T.; Bao, J. K.; Liu, Y.; Sun, Y. L.; Ablimit, A.; Zhai, H. F.; Jiang, H.; Feng, C. M.; Xu, Z. A.; Cao, G. H. Unconventional Superconductivity in Quasi-One-Dimensional $Rb_2Cr_3As_3$. *Phys. Rev. B* **2015**, *91*, No. 020506.

(3) Mu, Q. G.; Ruan, B. B.; Pan, B. J.; Liu, T.; Yu, J.; Zhao, K.; Chen, G. F.; Ren, Z. A. Ion-Exchange Synthesis and Superconductivity at 8.6 K of $Na_2Cr_3As_3$ with Quasi-One-Dimensional Crystal Structure. *Phys. Rev. Mater.* **2018**, *2*, No. 034803.

(4) Mu, Q. G.; Ruan, B. B.; Pan, B. J.; Liu, T.; Yu, J.; Zhao, K.; Chen, G. F.; Ren, Z. A. Superconductivity at 5 K in Quasi-One-Dimensional Cr-Based KCr_3As_3 Single Crystals. *Phys. Rev. B* **2017**, *96*, No. 140504.

(5) Bao, J. K.; Liu, J. Y.; Ma, C. W.; Meng, Z. H.; Tang, Z. T.; Sun, Y. L.; Zhai, H. F.; Jiang, H.; Bai, H.; Feng, C. M.; Xu, Z. A.; Cao, G. H. Superconductivity in Quasi-One-Dimensional $K_2Cr_3As_3$ with Significant Electron Correlations. *Phys. Rev. X* **2015**, *5*, No. 011013.

(6) Wu, W.; Cheng, J.; Matsubayashi, K.; Kong, P.; Lin, F.; Jin, C.; Wang, N.; Uwatoko, Y.; Luo, J. Superconductivity in the Vicinity of Antiferromagnetic Order in CrAs. *Nat. Commun.* **2014**, *5*, No. 5508.

(7) Tang, Z.-T.; Bao, J.-K.; Wang, Z.; Bai, H.; Jiang, H.; Liu, Y.; Zhai, H.-F.; Feng, C.-M.; Xu, Z.-A.; Cao, G.-H. Superconductivity in Quasi-One-Dimensional $Cs_2Cr_3As_3$ with Large Interchain Distance. *Sci. China Mater.* **2015**, *58*, 16−20.

(8) Shen, Y.; Wang, Q.; Hao, Y.; Pan, B.; Feng, Y.; Huang, Q.; Harriger, L. W.; Leao, J. B.; Zhao, Y.; Chisnell, R. M.; Lynn, J. W.; Cao, H.; Hu, J.; Zhao, J. Structural and Magnetic Phase Diagram of CrAs and Its Relationship with Pressure-Induced Superconductivity. *Phys. Rev. B* **2016**, *93*, No. 060503.

(9) Wu, X. X.; Le, C. C.; Yuan, J.; Fan, H.; Hu, J. P. Magnetism in Quasi-One-Dimensional $A_2Cr_3As_3$ (A = K, Rb) Superconductors. *Chin. Phys. Lett.* **2015**, *32*, No. 057401.

(10) Das, P.; Sangeetha, N. S.; Lindemann, G. R.; Heitmann, T. W.; Kreyssig, A.; Goldman, A. I.; McQueeney, R. J.; Johnston, D. C.; Vaknin, D. Itinerant G-Type Antiferromagnetic Order in $SrCr_2As_2$. *Phys. Rev. B* **2017**, *96*, No. 014411.

(11) Paramanik, U. B.; Prasad, R.; Geibel, C.; Hossain, Z. Itinerant and Local-Moment Magnetism in $EuCr_2As_2$ Single Crystals. *Phys. Rev. B* **2014**, *89*, No. 144423.

(12) Singh, D. J.; Sefat, A. S.; McGuire, M. A.; Sales, B. C.; Mandrus, D.; Vanbebber, L. H.; Keppens, V. Itinerant Antiferromagnetism in $BaCr_2As_2$: Experimental Characterization and Electronic Structure Calculations. *Phys. Rev. B* **2009**, *79*, No. 094429.

(13) Duan, L.; Wang, X. C.; Zhang, J.; Zhao, J. F.; Zhao, Z.; Xiao, C.; Guan, C.; Wang, S.; Shi, L.; Zhu, J.; Jin, C. Q. Critical Behavior of the Ferromagnetic Metal La_3CrAs_5 with Quasi-One-Dimensional Spin Chains. *J. Alloys Compd.* **2022**, *905*, No. 164214.

(14) Ovchinnikov, A.; Smetana, V.; Mudring, A. V. Metallic Alloys at the Edge of Complexity: Structural Aspects, Chemical Bonding and Physical Properties. *J. Phys.: Condens. Matter* **2020**, *32*, No. 243002.

(15) Dolomanov, O. V.; Bourhis, L. J.; Gildea, R. J.; Howard, J. A. K.; Puschmann, H. OLEX2: A Complete Structure Solution, Refinement and Analysis Program. *J. Appl. Crystallogr.* **2009**, *42*, 339−341.

(16) Sheldrick, G. M. Crystal Structure Refinement with SHELXL. *Acta Crystallogr., Sect. C: Struct. Chem.* **2015**, *71*, 3−8.

(17) Sheldrick, G. M. SHELXT − Integrated Space-Group and Crystal-Structure Determination. *Acta Crystallogr., Sect. A: Found. Adv.* **2015**, *71*, 3−8.

(18) Gelato, L. M.; Parthé, E. STRUCTURE TIDY − a Computer Program to Standardize Crystal Structure Data. *J. Appl. Crystallogr.* **1987**, *20*, 139−143.

(19) Jepsen, O.; Andersen, O. K. *The Stuttgart TB-LMTO-ASA Program*, Version 4.7; Max-Planck-Institut für Festkörperforschung: Stuttgart, Germany.

(20) Andersen, O. K.; Jepsen, O. Explicit, First-Principles Tight Binding Theory. *Phys. Rev. Lett.* **1984**, *53*, 2571−2574.

(21) Barth, U. v.; Hedin, L. A Local Exchange-Correlation Potential for the Spin Polarized Case. I. *J. Phys. C: Solid State Phys.* **1972**, *5*, 1629−1642.

(22) Jeitschko, W.; Donohue, P. C. High-Pressure CrP_2 and $CrAs_2$ with $OsGe_2$ -Type Structure and Crystal Chemistry of Transition-Metal Dipnictides. *Acta Crystallogr., Sect. B: Struct. Crystallogr. Cryst. Chem.* **1973**, *29*, 783−789.

(23) Baurecht, H. E.; Boller, H.; Nowotny, H. Die Kristallstruktur Des Chromarsenids Cr_4As_3. *Monatsh. Chem.* **1970**, *101*, 1696−1703.

(24) Berger, R. The Crystal Structure of β-V_5As_3, γ-V_5As_3 and Cr_5As_3. *Acta Chem. Scand. A* **1976**, *30*, 363−369.

(25) Jeitschko, W.; Johnson, V. High Pressure Mn_2As with Fe_2P-Type Structure. *Acta Crystallogr., Sect. B: Struct. Crystallogr. Cryst. Chem.* **1972**, *28*, 1971−1973.

(26) Venkatraman, M.; Neumann, J. P. The As-Cr (Arsenic-Chromium) system. *Bull. Alloy Phase Diagrams* **1990**, *11*, 424−430.

(27) Boller, H.; Wolfsgruber, H.; Nowotny, H. X-ray investigations in the chromium-silicon (germanium)-arsenic systems. *Monatsh. Chem.* **1967**, *98*, 2356−2361.

(28) Carter, F. L.; Calvert, L. D. The Crystal Chemistry of the Europium Arsenides. In *The Rare Earths in Modern Science and Technology*; McCarthy, G. J.; Silber, H. B.; Rhyne, J. J.; Kalina, F. M., Eds.; Springer: Boston, MA, 1982.

(29) Ono, S.; Hui, F. L.; Despault, J. G.; Calvert, L. D.; Taylor, J. B. X-ray investigations in the chromium-silicon (germanium)-arsenic systems. *J. Less-Common Met.* **2003**, *25*, 287−294.

(30) Leon-Escamilla, E. A.; Hurng, W.-M.; Peterson, E. S.; Corbett, J. D. Synthesis, Structure, and Properties of $Ca_{16}Sb_{11}$, a Complex Zintl Phase. Twelve Other Isotypic Compounds Formed by Divalent Metals and Pnictogens. *Inorg. Chem.* **1997**, *36*, 703−710.

(31) Chattopadhyay, T.; Brown, P. J.; Thalmeier, P.; Bauhofer, W.; von Schnering, H. G. Neutron-Diffraction Study of the Magnetic Ordering in $EuAs_3$, $Eu(As_{1-x}P_x)_3$, and β-EuP_3. *Phys. Rev. B* **1988**, *37*, 269−282.

(32) Wang, Y.; Calvert, L. D.; Gabe, E. J.; Taylor, J. B. Structure of Europium Arsenide Eu_5As_4: A More Symmetrical Version of the Sm_5Ge_4-Type Structure. *Acta Crystallogr., Sect. B: Struct. Crystallogr. Cryst. Chem.* **1978**, *34*, 1962−1965.

(33) Wang, Y.; Calvert, L. D.; Taylor, J. B. The Structures of Eu_4As_3 and La_4Sb_3. *Acta Crystallogr., Sect. B: Struct. Crystallogr. Cryst. Chem.* **1980**, *36*, 221−222.

(34) Iandelli, A.; Franceschi, E. On the Crystal Structure of the Compounds CaP, SrP, CaAs, SrAs and EuAs. *J. Less-Common Met.* **1973**, *30*, 211−216.

(35) Wang, Y.; Calvert, L. D.; Gabe, E. J.; Taylor, J. B. Structure of Two Forms of Europium Arsenide Eu_5As_3. *Acta Crystallogr., Sect. B: Struct. Crystallogr. Cryst. Chem.* **1978**, *34*, 2281−2284.

(36) Ono, S.; Hui, F. L.; Despault, J. G.; Calvert, L. D.; Taylor, J. B. Rare-Earth Pnictides: The Arsenic-Rich Europium Arsenides. *J. Less-Common Met.* **1971**, *25*, 287−294.

(37) Wang, A.; Baranets, S.; Liu, Y.; Tong, X.; Stavitski, E.; Zhang, J.; Chai, Y.; Yin, W. G.; Bobev, S.; Petrovic, C. Magnetic mixed valent semimetal $EuZnSb_2$ with Dirac states in the band structure. *Phys. Rev. Res.* **2020**, *2*, No. 033462.

https://doi.org/10.1021/acs.chemmater.5c02660
Chem. Mater. 2025, 37, 9597−9608

(38) Shannon, R. D. Revised effective ionic radii and systematic studies of interatomic distances in halides and chalcogenides. *Acta Crystallogr., Sect. A* **1976**, *32*, 751.
(39) Verma, A.; Li, J.; Subramanian, M. A. Cr^{2+} in Square Planar Coordination: Durable and Intense Magenta Pigments Inspired by Lunar Mineralogy. *Chem. Mater.* **2024**, *36*, 3837−3843.
(40) Cordero, B.; Gómez, V.; Platero-Prats, A. E.; Revés, M.; Echeverría, J.; Cremades, E.; Barragán, F.; Alvarez, S. Covalent Radii Revisited. *Dalton Trans.* **2008**, *21*, 2832−2838.
(41) Anisimov, V. I.; Aryasetiawan, F.; Lichtenstein, A. I. First-principles calculations of the electronic structure and spectra of strongly correlated systems: the LDA+*U* method. *J. Phys.: Condens. Matter* **1997**, *9*, 767−808.
(42) Ishtiyak, M.; Watts, S. P.; Thipe, B.; Womack, F.; Adams, P.; Bai, X.; Young, D. P.; Bobev, S.; Baranets, S. Advancing Heteroanionicity in Zintl Phases: Crystal Structures, Thermoelectric and Magnetic Properties of Two Quaternary Semiconducting Arsenide Oxides, $Eu_8Zn_2As_6O$ and $Eu_{14}Zn_5As_{12}O$. *Inorg. Chem.* **2024**, *63*, 20226−20239.
(43) Michels, G.; Junk, S.; Lossau, N.; Schlabitz, W.; Wohlleben, D.; Johrendt, D.; Mewis, A.; Sauer, C.; Woike, T. Mixed valency and first order phase transition in EuPdAs. *Z. Phys. B: Condens. Matter* **1992**, *86*, 53−58.
(44) Brown, I. D. Recent Developments in the Methods and Applications of the Bond Valence Model. *Chem. Rev.* **2009**, *109* (12), 6858−6919.
(45) https://www.iucr.org/resources/data/data-sets/bond-valence-parameters (accessed July 22, 2025).
(46) Nandi, S.; Xiao, Y.; Qureshi, N.; Paramanik, U. B.; Jin, W. T.; Su, Y.; Ouladdiaf, B.; Hossain, Z.; Bruckel, T. Magnetic structures of the Eu and Cr moments in $EuCr_2As_2$: Neutron diffraction study. *Phys. Rev. B* **2016**, *94*, No. 094411.
(47) Xu, X.; Jones, M. A.; Cassidy, S. J.; Manuel, P.; Orlandi, F.; Batuk, M.; Hadermann, J.; Clarke, S. J. Magnetic Ordering in the Layered Cr(II) Oxide Arsenides $Sr_2CrO_2Cr_2As_2$ and $Ba_2CrO_2Cr_2As_2$. *Inorg. Chem.* **2020**, *59*, 15898−15912.
(48) Jiang, H.; Bao, J.-K.; Zhai, H.-F.; Tang, Z.-T.; Sun, Y.-L.; Liu, Y.; Wang, Z.-C.; Bai, H.; Xu, Z.-A.; Cao, G. H. Physical properties and electronic structure of $Sr_2Cr_3As_2O_2$ containing CrO_2 and Cr_2As_2 square-planar lattices. *Phys. Rev. B* **2015**, *92*, No. 205107.
(49) Sobczak, R. Magnetische Untersuchungen an den ferromagnetischen Chromarseniden (Cr ≈ 0.60, As ≈ 0.40). *Monatsh. Chem.* **1974**, *105*, 1067−1070.
(50) https://docs.scipy.org/doc/scipy/reference/optimize.html (accessed July 22, 2025).
(51) https://pymoo.org/algorithms/soo/cmaes.html (accessed July 22, 2025).
(52) Ogunbunmi, M. O.; Bobev, S. Observation of Anomalously High Seebeck Coefficients in the Family of Zintl Phase Semiconductors $Ca_{10}RECdSb_9$ (*RE* = Rare-Earth Metal). *Chem. Mater.* **2022**, *34*, 8808−8814.
(53) Goldsmid, H. J. *Introduction to Thermoelectricity*; Springer Berlin Heidelberg: Berlin, Heidelberg, 2016; Vol. *121*.
(54) Pinsard-Gaudart, L.; Bérardan, D.; Bobroff, J.; Dragoe, N. Large Seebeck coefficients in iron-oxypnictides: a new route towards *n*-type thermoelectric materials. *Phys. Status Solidi RRL* **2008**, *2*, 185−187.
(55) Zingl, M.; Kraberger, G. J.; Aichhorn, M. Thermopower of the electron-doped manganese pnictide LaMnAsO. *Phys. Rev. Mater.* **2019**, *3*, No. 075404.
(56) Wu, S.-Q.; Wang, Z.-C.; He, C.-Y.; Tang, Z.-T.; Liu, Y.; Cao, G.-H. Superconductivity at 33−37 K in $ALn_2Fe_4As_4O_2$ (*A* = K and Cs; *Ln* = lanthanides). *Phys. Rev. Mater.* **2017**, *1*, No. 044804.
(57) Boeri, L.; Dolgov, O. V.; Golubov, A. A. Is $LaFeAsO_{1-x}F_x$ an Electron-Phonon Superconductor? *Phys. Rev. Lett.* **2008**, *101*, No. 026403.
(58) Wood, C. Materials for Thermoelectric Energy Conversion. *Rep. Prog. Phys.* **1988**, *51* (4), 459−539.
(59) Ogunbunmi, M. O.; Baranets, S.; Bobev, S. Structural Complexity and Tuned Thermoelectric Properties of a Polymorph of the Zintl Phase Ca_2CdSb_2 with a Non-Centrosymmetric Monoclinic Structure. *Inorg. Chem.* **2022**, *61*, 10888−10897.
(60) Ghosh, K.; Borgsmiller, L.; Baranets, S.; Snyder, G. J.; Bobev, S. Thermoelectric Zintl phases with ultralow thermal conductivity: synthesis, structural characterization, and transport properties of $Ca_{10}AlSb_9$ and $Ca_{10}CdSb_9$. *J. Mater. Chem. A* **2024**, *12*, 25416−25428.
(61) Ogunbunmi, M. O.; Ghosh, K.; Donnelly, C.; Baranets, S.; Bobev, S. The Zintl pnictides $Yb_{10}CdSb_9$ and $Yb_{14}CdSb_{11}$: New candidate thermoelectric materials. *J. Appl. Phys.* **2025**, *137*, 1635021−1635025.
(62) Snyder, G. J.; Toberer, E. S. Complex Thermoelectric Materials. *Nat. Mater.* **2008**, *7* (2), 105−114.
(63) Ogunbunmi, M. O.; Baranets, S.; Bobev, S. Synthesis and Transport Properties of the Family of Zintl Phases Ca_3RESb_3 (*RE* = La−Nd, Sm, Gd−Tm, Lu): Exploring the Roles of Crystallographic Disorder and Core 4*f* Electrons for Enhancing Thermoelectric Performance. *Chem. Mater.* **2021**, *33*, 9382−9392.
(64) Vaney, J.-B.; Yamini, S. A.; Takaki, H.; Kobayashi, K.; Kobayashi, N.; Mori, T. Magnetism-Mediated Thermoelectric Performance of the Cr-Doped Bismuth Telluride Tetradymite. *Mater. Today Phys.* **2019**, *9*, No. 100090.
(65) Zhao, C.-C.; Xiao, C. When Thermoelectric Materials Come across with Magnetism. *Rare Met.* **2021**, *40*, 752−766.

https://doi.org/10.1021/acs.chemmater.5c02660
Chem. Mater. 2025, 37, 9597−9608